Graphene Assembly

DOI: 10.1002/anie.201006240

Three-Dimensional Self-Assembly of Graphene Oxide Platelets into Mechanically Flexible Macroporous Carbon Films**

*Sun Hwa Lee, Hyun Wook Kim, Jin Ok Hwang, Won Jun Lee, Joon Kwon, Christopher W. Bielawski, Rodney S. Ruoff, and Sang Ouk Kim**

Graphene is an atom-thick, two-dimensional material comprised of a monolayer hexagonal sp^2-hybridized carbons.[1,2] It is flexible, has a large specific surface area, and exhibits excellent electrical and thermal conductivities and also good mechanical properties. Moreover, given the low cost of natural graphite, the potential for obtaining large quantities of graphene by a low-cost production process is high. As such, graphene and its chemically modified forms[3] are promising building blocks for accessing highly ordered assemblies that are suitable for nanoelectronics, energy storage/conversion, catalysis, composites, and other applications.[1–8] Although previous efforts have demonstrated that graphene-based platelets may be assembled into papers, thin films, or other two-dimensional constructs,[9–13] the ability to control the assembly such platelets into three-dimensional (3D) structures could result in the carbon materials that exhibit very large surface areas, unusual or novel physical and electronic properties, unsurpassed chemical functionality, and other attractive features that are necessary for the aforementioned applications.[3,14–16]

Herein we demonstrate the self-assembly of graphene oxide (GO) platelets into mechanically flexible, macroporous 3D carbon films with tunable porous morphologies. Self-assembly is the spontaneous bottom-up organization of pre-existing components into patterned structures.[17,18] The intrinsic parallelism and scalability inherent to self-assembly can, in principle, enable low-cost, large-scale syntheses of highly ordered nanostructures.[19–25] Indeed, as will be described below, the self-assembly of chemically modified graphene platelets into a complex 3D morphology was achieved by the "breath-figure" method, which is a straightforward procedure for synthesizing large-area porous polymer films.[25–34]

The breath-figure method as employed herein is illustrated in Figure 1 A. Briefly, polymer-grafted GO platelets were synthesized and dispersed in an organic solvent. The dispersion was then cast onto a suitable substrate and exposed to a stream of humid air. Endothermic evaporation of the volatile organic solvent resulted in the spontaneous conden-

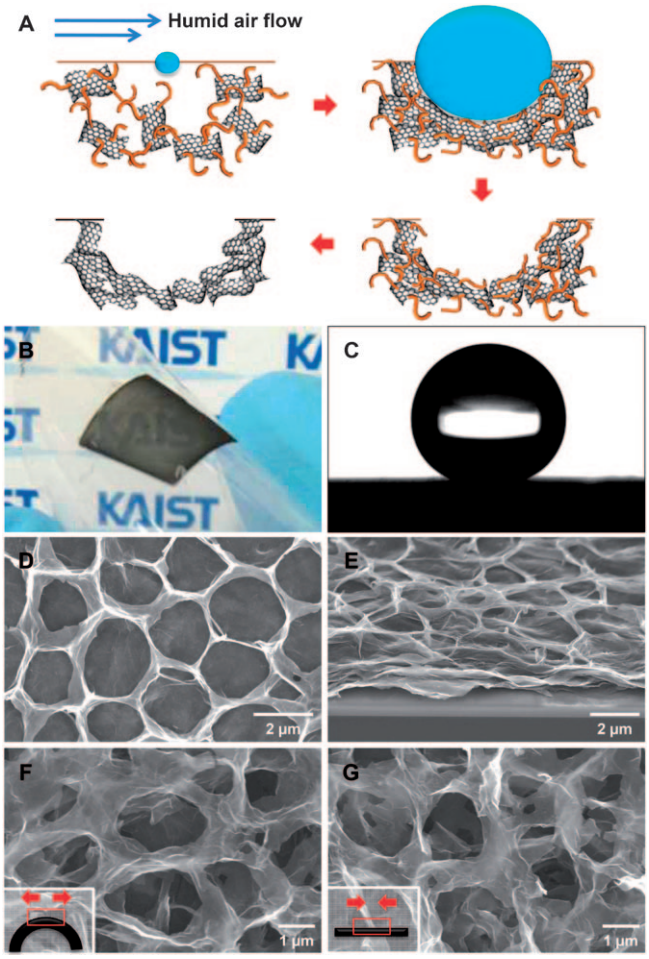

Figure 1. A) Procedure for the self-assembly of RGO into macroporous carbon films. B) A photograph of a mechanically flexible, semi-transparent macroporous RGO film on PET. C) A water contact angle of 152° was measured for the superhydrophobic macroporous RGO film. D) Plane-view and E) 60°-tilted SEM images of an RGO film. F,G) Plane-view SEM images of porous RGO film upon (F) and after (G) deformation.

[*] S. H. Lee, H. W. Kim, J. O. Hwang, W. J. Lee, J. Kwon, Prof. S. O. Kim
Department of Materials Science and Engineering, KAIST
Daejeon, 305-701 (Republic of Korea)
Fax: (+82) 42-350-3310
E-mail: sangouk.kim@kaist.ac.kr
Prof. C. W. Bielawski
Department of Chemistry and Biochemistry
The University of Texas at Austin
1 University Station, A5300, Austin, TX 78712-0165 (USA)
Prof. R. S. Ruoff
Department of Mechanical Engineering and
the Texas Materials Institute, The University of Texas at Austin
204 East Dean Keeton St., Austin, TX 78712-0292 (USA)

[**] This work was supported by the National Research Laboratory Program (R0A-2008-000-20057-0) and Converging Research Center Program (2009-0093659), and the World Premier Materials (WPM) program (10037689) funded by the Korean government.

Supporting information for this article is available on the WWW under http://dx.doi.org/10.1002/anie.201006240.

sation and close packing of aqueous droplets at the organic solution surface. Subsequent drying resulted in a macroporous film of polymer-grafted GO on the substrate which, upon pyrolysis, afforded a mechanically flexible and robust macroporous films comprised of reduced graphene oxide (RGO) platelets. Building on this method, we found that nitrogen doping (N-doping) of the 3D assemblies of RGO provided materials with improved electrical properties and high chemical reactivity.

The polymer-grafted GO platelets were prepared using a previously reported procedure[35] by surface-initiated atom transfer radical polymerization (ATRP).[36] The GO platelets obtained contained approximately one initiator per 66 carbon atoms (that is, one initiator per 1.54 nm^2; see the Supporting Information, Table S1). These polystyrene-grafted graphene oxide (PS-GO) platelets were found to readily disperse in benzene; as described below, this feature was used to achieve 3D macroporous assemblies of RGO platelets by pyrolysis of PS-GO.

As shown in Figure 1B, drop-casting a dispersion of PS-GO/benzene (5 mg mL^{-1}) onto a SiO_2 substrate afforded a mechanically flexible macroporous film after solvent evaporation, which was transferable to a flexible poly(ethylene terephalate) (PET) film. Despite the micrometer-scale thickness (ca. 3.8 μm), the assembled macroporous film was only semi-transparent. Regardless, subsequent pyrolysis of the film facilitated the thermal reduction of the GO platelets and afforded a film that was determined to be superhydrophobic (Figure 1C)[37] an attractive property that may result from their unique morphologies (see below).

Scanning electron microscopy (SEM) images of the microscale morphology of the aforementioned macroporous assembly of RGO platelets are shown in Figure 1D,E. The plane-view shows a few closely packed macropores with a nanoscale rim thickness (Figure 1D). The 60° tilt image of a fractured sample reveals open porous morphology (Figure 1E). The RGO assembly is mechanically flexible and conforms to flexible substrates, even upon deformation. Figure 1F shows a plane-view SEM image of a concave film with a radius of curvature of about 2 mm. In this case, the pores are slightly elongated, but the macropore morphology is well-maintained. When the film is restored to its original planar geometry (Figure 1G), the macropores also recover their initial shapes.

The detailed nanoscale morphology of these films was investigated further by high-magnification SEM and transmission electron microscopy (TEM). Figure 2A shows a high magnification SEM image of the interconnected rim structure. The rims, composed of stacked and overlapped RGO platelets, are highly wrinkled along the boundary of macropores. The wrinkling presumably occurs upon the growth of the aqueous droplets during the breath-figure process, or during the shrinkage of the film that occurs upon the pyrolysis of the polymer matrix, or both. Although the thickness of the macroporous film typically decreased by 21% after pyrolysis of the grafted polymers, the porous morphology is well-maintained (Supporting Information, Figure S3). TEM images (Figure 2B,C) also reveal a wrinkled conformation of RGO platelets. The average interlayer spacing of the RGO

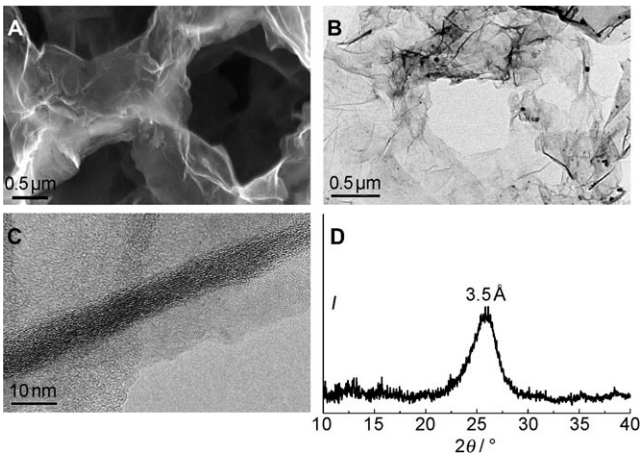

Figure 2. Microstructure of various macroporous RGO films. A) SEM image of RGO sheets around the pores. B,C) Low- and high-magnification TEM images of porous RGO assembly. The RGO platelets surrounding the pores were pushed and wrinkled by growth of aqueous droplets and volume reduction through pyrolysis. D) XRD spectra of a porous RGO film, showing the interlayer spacing of about 3.5 Å.

platelets was measured to be about 3.5 Å by X-ray diffraction (XRD), which is slightly larger than the interlayer spacing in graphite (3.35 Å).[38] Using Scherrer's equation, these films were estimated to have an average of 5–15 wrinkled layers.[39,40]

Controlling the pore size and the number of pore layers was achieved by changing the concentration of precursor solution and the chain length of grafted polymers at the GO platelet surface. PS-GO with different polymer lengths was prepared by varying the initial monomer to initiator ratio. For example, loading 1 g of initiator modified GO with 5 mL or 2.5 mL of styrene monomer afforded PS-GO-5 containing 18 wt% of GO or PS-GO-2.5 with 58 wt% of GO content, respectively, after polymerization (Supporting Information, Figure S4). The weight-average molecular weights of the grafted polystyrene were measured by gel permeation chromatography to be 17600 g mol^{-1} for PS-GO-2.5 and 26400 g mol^{-1} for PS-GO-5, respectively, after detaching the polymers by saponification (Supporting Information).[35] Although polymer chains of longer and shorter lengths than those described above were also explored, deleterious results were obtained. For example, when the grafted polymer length was shorter than that contained in PS-GO-2.5, the respective polymer grafted GO platelets were not dispersible in benzene. In contrast, when the grafted polymer chains were longer than those found in PS-GO-5, the resulting films exhibited limited porosity, most likely because the polymer chains were too long to facilitate self-assembly of the GO platelets.

Using the aforementioned film-forming procedures, the self-assembly of PS-GO-5 resulted in monolayer macroporous morphologies. When a dispersion of PS-GO-5 in benzene was prepared at 3 mg mL^{-1}, the resulting film exhibited hexagonal-shaped pores with an average size of 3.7 μm (Figure 3B). However, when the concentration of PS-

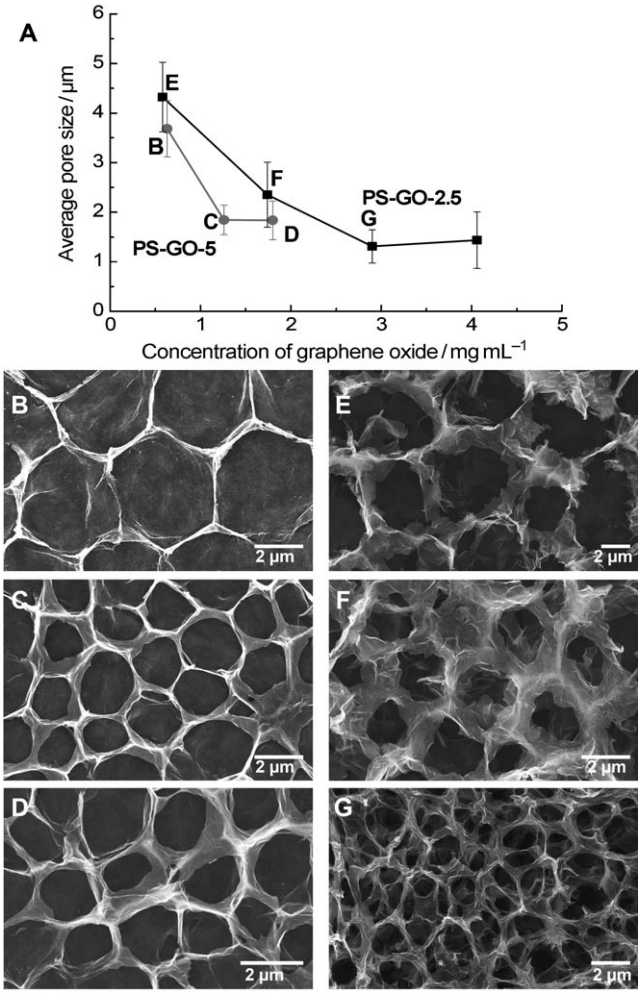

Figure 3. Control of pore size and number of pore layers of macroporous RGO films. A) The average pore sizes versus GO concentration in PS-GO for various chain lengths of grafted polymers. B–D) SEM images of porous films from PS-GO-5 at concentrations of 3.5 (0.63), 7 (1.26), and 10 (1.80) mg mL^{-1}. E–G) SEM images of porous films from PS-GO-2.5 at concentrations of 1 (0.58), 3 (1.74), and 5 (2.90) mg mL^{-1}. The numbers in parentheses denote the concentration of GO in each of the PS-GO solutions.

GO-5 was increased to 7 mg mL^{-1} or 10 mg mL^{-1}, the resulting films exhibited smaller pores with irregular shapes. For example, using 10 mg mL^{-1} dispersion, the average pore size in the respective film was measured at 1.8 μm (Figure 3C,D). As the GO platelet concentration was increased further, the precursor solution became viscous such that the growth of aqueous droplets was hindered.

The assembly of PS-GO-2.5 generated multilayered open porous structures (see Figure 3E–G). As the concentration of PS-GO-2.5 increased from 1 mg mL^{-1} to 3, 5, and 7 mg mL^{-1}, the average pore size systematically decreased from 4.3 μm to 1.4 μm. A correlation between the average pore sizes with the contents of GO employed in the respective dispersions for different chain lengths of polymers grafted to the GO is shown in Figure 3A. In general, the films prepared from PS-GO-2.5 afforded larger pores than those prepared from PS-GO-5 over the entire range of GO platelet concentration studied.

The chemical functionality and electrical properties of such films could be enhanced by N-doping. After formation of macroporous RGO films using the procedures described above, they were heated at 1000 °C for 5 min in a mixture of NH_3 (60 sccm) and H_2 (40 sccm) at 0.9 Torr. No noticeable change between GO and the samples after thermal treatment was seen in the Raman spectra, though porous RGO samples underwent thermal treatment at high temperatures (Supporting Information, Figure S5A). The G/D ratio of porous RGO films was 0.99, which is not a dramatic change from that of GO (0.84). However, a C–N bond was observed in the C1s X-ray photoelectron spectra in the sample that was treated with NH_3, which was (Supporting Information, Figure S5B), in contrast with the films obtained after pyrolysis or heated under H_2 (no NH_3). Moreover, a strong signal was detected in the N1s XPS spectrum after NH_3 treatment, confirming that nitrogen was successfully incorporated into the assembly (Supporting Information, Figure S5C).[41] The sample was determined by XPS to contain 11 % nitrogen.

It is well-known that GO is an electrical insulator owing to the presence of oxygen functional groups on their basal planes and edges. To enhance the electrical properties of GO, several reduction procedures have been developed, including thermal, chemical, and electrochemical method.[3,42,43] Among them, simple pyrolysis in conjunction with N-doping process was found to significantly enhance the electrical properties of GO. Figure 4A compares the *I–V* curves of macroporous RGO films before and after pyrolysis or post-thermal reduction. The curves were measured at room temperature by Van der Paw method showed typical linear ohmic behaviors, except for the insulating behavior of GO before pyrolysis. The surface resistance of the macroporous RGO film reduced during the pyrolysis of grafted polymers was approximately 128.2 Ω. Further N-doping decreased the resistances of macroporous film to 13.4 Ω, which corresponds to an electrical conductivity of 649 S cm^{-1} (film thickness: 1.15 μm).

As it is well-known that the pyridinic, pyrrolic, or graphitic nitrogen atoms doped in graphene can serve as reduction and coordination sites for metal salts,[44–46] we reasoned that the aforementioned macroporous RGO assemblies doped with nitrogen could function similarly. Moreover, we reasoned that the chemical reactivity may be enhanced by the improved wettability exhibited by the N-doped material (Supporting Information, Figure S2B). Indeed, immersion of the N-doped material in a gold salt aqueous solution ($HAuCl_4$, 10 mM) afforded flower-like gold particles on the surface (Figure 4B). As illustrated in Figure 4C, we believe that these particles were nucleated at the N-doped sites and grew by the spontaneous reduction of gold ions. The nucleation and growth of the flower-like gold particles occurred at room temperature without additional reducing agents. The wrinkled morphology of the macroporous RGO assembly appeared to be critical for the flower-like morphologies observed. Treatment of planar N-doped RGO films with the same aqueous gold solution afforded spherical nanoparticles (Supporting Information, Figure S5D,E).

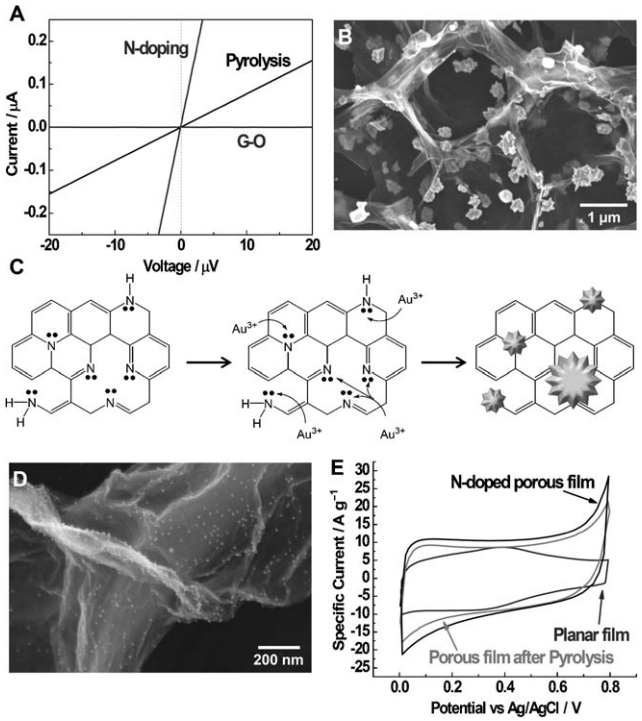

Figure 4. Electrical behavior, gold functionalization, and supercapacitor performance of N-doped macroporous RGO films. A) *I–V* characteristics of GO and macroporous RGO films before and after thermal treatment. Thermal treatments could improve the electrical conductivities of GO films. B) SEM image of flower-like gold particles grown from N-doped macroporous RGO film. C) Nucleation and growth of gold particles on N-doped graphene. D) SEM image of the N-doped porous RGO assembly decorated with gold nanoparticles by ionic interaction. E) Supercapacitor performance of macroporous RGO films. N-doped porous RGO film showing high specific capacitance owing to a large surface area and high electrical conductivity.

Along with the spontaneous reduction of metal salts, water dispersible metal nanoparticles were also functionalized at the surface of N-doped RGO assembly. Figure 4D shows a macroporous RGO assembly decorated with 10 nm-sized gold nanoparticles (see Experimental Section in the Supporting Information). These gold nanoparticles contained terminal carboxylates, which we believe is coordinated to the protonated N-doped sites of RGO by an electrostatic interaction (Supporting Information, Figure S6). The uniform distribution of metal particles over the entire RGO assembly results from the N-doping throughout the basal plane and also the edge of the RGO platelet.

Taking advantage of the large surface areas and high electrical conductivities of the macroporous RGO films, these materials were investigated for their potential in supercapacitor applications. As shown in Figure 4E, the cyclic voltammograms (CVs) of pyrolyzed or N-doped films exhibited a rectangular shape at a high scan rate of $100\,mV\,s^{-1}$ over a potential range of 0–0.8 V, which is consistent with good charge propagation at the electrodes.[5] The specific capacitances of the as-pyrolyzed and N-doped macroporous RGO assemblies were measured to be $86.7\,F\,g^{-1}$ and $103.2\,F\,g^{-1}$ in 1M aqueous H_2SO_4 aqueous solution, respectively. In contrast, the capacitance from an electrode that was prepared from a planar RGO electrode was measured at $62.9\,F\,g^{-1}$. The enhanced specific capacitance of the former was attributed to the improved surface area of 3D macroporous assembly and high electrical conductivity and good wettability enabled by N-doping.

In summary, we have demonstrated a straightforward self-assembly method to fabricate highly ordered, mechanically flexible macroporous RGO assemblies with tunable open porous morphologies. The pore size and the number of porous layers were effectively controlled by the concentration of the organic precursor disperson and the length of polymer chains grafted to the GO surface. Additional N-doping of these 3D carbon assemblies enhanced their electrical conductivities and facilitated further chemical functionalization under mild aqueous-based processes. Our facile preparation of highly ordered macroporous graphene film may find utility in various applications, including energy storage/conversion, biological scaffold, supporting frameworks of catalyst, and sensors.

Received: October 5, 2010
Published online: November 29, 2010

Keywords: flexible materials · graphene · porosity · self-assembly · thin films

[1] A. K. Geim, K. S. Novoselov, *Nat. Mater.* **2007**, *6*, 183.
[2] Y. Zhu, S. Murali, W. Cai, X. Li, J. W. Suk, J. R. Potts, R. S. Ruoff, *Adv. Mater.* **2010**, *22*, 3906.
[3] S. Park, R. S. Ruoff, *Nat. Nanotechnol.* **2009**, *4*, 217.
[4] C. Lee, X. Wei, J. W. Kysar, J. Hone, *Science* **2008**, *321*, 385.
[5] M. D. Stoller, S. Park, Y. Zhu, J. An, R. S. Ruoff, *Nano Lett.* **2008**, *8*, 3498.
[6] S. Stankovich, D. A. Dikin, G. H. B. Dommett, K. M. Kohlhaas, E. J. Zimney, E. A. Stach, R. D. Piner, S. T. Nguyen, R. S. Ruoff, *Nature* **2006**, *442*, 282.
[7] D. R. Dreyer, S. Park, C. W. Bielawski, R. S. Ruoff, *Chem. Soc. Rev.* **2010**, *39*, 228.
[8] V. C. Tung, M. J. Allen, Y. Yang, R. B. Kaner, *Nat. Nanotechnol.* **2009**, *4*, 25.
[9] D. A. Dikin, S. Stankovich, E. J. Zimney, R. D. Piner, G. H. B. Dommett, G. Evmenenko, S. T. Nguyen, R. S. Ruoff, *Nature* **2007**, *448*, 457.
[10] G. Eda, G. Fanchini, M. Chhowalla, *Nat. Nanotechnol.* **2008**, *3*, 270.
[11] D. H. Lee, J. E. Kim, T. H. Han, J. W. Hwang, S. W. Jeon, S.-Y. Choi, S. H. Hong, W. J. Lee, R. S. Ruoff, S. O. Kim, *Adv. Mater.* **2010**, *22*, 1247.
[12] G. Eda, M. Chhowalla, *Adv. Mater.* **2010**, *22*, 2392.
[13] B. H. Kim, J. Y. Kim, S. J. Jeong, J. O. Hwang, D. H. Lee, D. O. Shin, S. Y. Choi, S. O. Kim, *ACS Nano* **2010**, *4*, 5464.
[14] J. R. Lomeda, C. D. Doyle, D. V. Kosynkin, W. F. Hwang, J. M. Tour, *J. Am. Chem. Soc.* **2008**, *130*, 16201.
[15] X. An, T. Simmons, R. Shah, C. Wolfe, K. M. Lewis, M. Washington, S. K. Nayak, S. Talapatra, S. Kar, *Nano Lett.* **2010**, DOI: 10.1021/nl903557p.
[16] E.-Y. Choi, T. H. Han, J. Hong, J. E. Kim, S. H. Lee, H. W. Kim, S. O. Kim, *J. Mater. Chem.* **2010**, *20*, 1907.
[17] G. M. Whitesides, B. Grzybowski, *Science* **2002**, *295*, 2418.
[18] G. M. Whitesides, M. Boncheva, *Proc. Natl. Acad. Sci. USA* **2002**, *99*, 69.

[19] C. M. Niemeyer, C. A. Mirkin, *Nanobiotechnology*, Wiley-VCH, Weinheim, **2004**.
[20] R. W. Kelsall, I. W. Hamley, M. J. Geoghegan, *Nanoscale Science and Technology*, Wiley, Chichester, **2005**.
[21] S. O. Kim, H. H. Solak, M. P. Stoykovich, N. J. Ferrier, J. J. de Pablo, P. F. Nealey, *Nature* **2003**, *424*, 411.
[22] T. H. Han, J. Kim, J. S. Park, H. Ihee and S. O. Kim, *Adv. Mater.* **2007**, *19*, 3924.
[23] T. H. Han, W. J. Lee, D. H. Lee, J. E. Kim, E.-Y. Choi, S. O. Kim, *Adv. Mater.* **2010**, *22*, 2060.
[24] S.-J. Jeong, J. E. Kim, H.-S. Moon, B. H. Kim, S. M. Kim, J.-B. Kim, S. O. Kim, *Nano Lett.* **2009**, *9*, 2300.
[25] S. H. Lee, J. S. Park, B. K. Lim, C. B. Mo, W. J. Lee, J. M. Lee, S. H. Hong, S. O. Kim, *Soft Matter* **2009**, *5*, 2343.
[26] G. Widawski, M. Rawiso, B. François, *Nature* **1994**, *369*, 387.
[27] H. Yabu, M. Shimomura, *Chem. Mater.* **2005**, *17*, 5231.
[28] B. K. Lim, S. H. Lee, J. S. Park, S. O. Kim, *Macromol. Res.* **2009**, *17*, 666.
[29] J. S. Park, S. H. Lee, T. H. Han, S. O. Kim, *Adv. Funct. Mater.* **2007**, *17*, 2315.
[30] A. Böker, Y. Lin, K. Chiapperini, R. Horowitz, M. Thompson, V. Carreon, T. Xu, C. Abetz, H. Skaff, A. D. Dinsmore, T. Emrick, T. P. Russell, *Nat. Mater.* **2004**, *3*, 302.
[31] H. Yabu, Y. Hirai, M. Shimomura, *Langmuir* **2006**, *22*, 9760.
[32] H. T. Ham, I. J. Chung, Y. S. Choi, S. H. Lee, S. O. Kim, *J. Phys. Chem. B* **2006**, *110*, 13959.
[33] H. Ejima, T. Iwata, N. Yoshie, *Macromolecules* **2008**, *41*, 9846.
[34] L. V. Gover, J. Parisi, *Z. Naturforsch. A* **2002**, *57*, 757.
[35] S. H. Lee, D. R. Dreyer, J. An, A. Velamakanni, R. D. Piner, S. Park, Y. Zhu, S. O. Kim, C. W. Bielawski, R. S. Ruoff, *Macromol. Rapid Commun.* **2010**, *31*, 281.
[36] K. Matyjaszewski, J. Xia, *Chem. Rev.* **2001**, *101*, 2921.
[37] L. Feng, S. Li, Y. Li, H. Li, L. Zhang, J. Zhai, Y. Song, B. Liu, L. Jiang, D. Zhu, *Adv. Mater.* **2002**, *14*, 1857.
[38] H. O. Pierson, *Handbook of Carbon, Graphite, Diamond, and Fullerenes: Properties, Processing and Applications*, Noyes Publications, New Jersey, **1993**.
[39] H. P. Klug, L. E. Alexander, *X-ray Diffraction Procedures*, Wiley, New York, **1959**.
[40] B. D. Cullity, S. R. Stock, *Elements of X-ray Diffraction*, 3rd ed., Prentice Hall, New Jersey, **2001**.
[41] L. S. Panchakarla, K. S. Subrahmanyam, S. K. Saha, A. Govindaraj, H. R. Krishnamurthy, U. V. Waghmare, C. N. R. Rao, *Adv. Mater.* **2009**, *21*, 4726.
[42] C. Mattevi, G. Eda, S. Agnoli, S. Miller, K. A. Mkhoyan, O. Celik, D. Mastrogiovanni, G. Granozzi, E. Garfunkel, M. Chhowalla, *Adv. Funct. Mater.* **2009**, *19*, 2577.
[43] S. J. An, Y. Zhu, S. H. Lee, M. D. Stoller, T. Emilsson, S. Park, A. Velamakanni, J. An, R. S. Ruoff, *J. Phys. Chem. Lett.* **2010**, *1*, 1259.
[44] D. Wei, Y. Liu, Y. Wang, H. Zhang, L. Huang, G. Yu, *Nano Lett.* **2009**, *9*, 1752.
[45] J. D. S. Newman, G. J. Blanchard, *Langmuir* **2006**, *22*, 5882.
[46] K. Gong, F. Du, Z. Xia, M. Durstock, L. Dai, *Science* **2009**, *323*, 760.

